Damage evolution in low-energy ion implanted silicon

R. Karmouch, Y. Anahory, J.-F. Mercure, D. Bouilly, M. Chicoine, G. Bentoumi, R. Leonelli, Y. Q. Wang, and F. Schiettekatte*

Regroupement Québécois sur les Matériaux de Pointe (RQMP), Département de Physique, Université de Montréal, Case Postale 6128 succursale Centre-ville, Montréal, Québec, Canada, H3C 3J7

(Received 1 November 2005; revised manuscript received 1 June 2006; published 5 February 2007)

The annealing of damage generated by low-energy ion implantation in polycrystalline silicon (poly-Si) and amorphous silicon (a-Si) is compared. The rate of heat release between implantation temperature and 350–500 °C for Si implanted in both materials and for different ions implanted in poly-Si shows a very similar shape, namely, a featureless signal that is characteristic of a series of processes continuously distributed in terms of activation energy. Nanocalorimetry signals differ only by their amplitude, a smaller amount of heat being released after light ion implantation compared to heavier ones for the same nominal number of displaced atoms. This shows the importance of dynamic annealing of the damage generated by light ions. A smaller amount of heat is released by implanted poly-Si compared to a-Si, underlining the effect of the surrounding crystal on the dynamic annealing and the relaxation of the defects. Damage accumulation after 30-keV Si implantation is also characterized by Raman scattering and reflectometry, featuring a similar trend in a-Si, poly-Si, and monocrystalline silicon (c-Si) with a saturation around 4 Si/nm^2. Considering these results together with other recent experiments in c-Si and molecular dynamic simulations, it is concluded that the damage generated by low-energy ion implantation that survives dynamic annealing is structurally very similar if not identical in both crystalline and amorphous silicon, giving rise to the same kind of processes during a thermal anneal. However, the damage peak obtained by channeling saturates only above 10 Si/nm^2. This suggests that between 4 and 10 Si/nm^2, further damage occurs by structural transformation without the addition of more stored energy.

DOI: 10.1103/PhysRevB.75.075304 PACS number(s): 61.72.Cc

I. INTRODUCTION

Ion implantation is a method of choice for introducing dopants in silicon and is often involved more than ten times in the fabrication process of microelectronic devices. Understanding damage annealing and defect evolution in the crystal after ion implantation is crucial as they dramatically influence dopant distribution and activation. Some phenomena such as the transient enhanced diffusion (TED)[1] are associated with excess interstitials[2] resulting from the implanted damage that, above a certain fluence threshold, aggregate into {311} rodlike and extended defects during the annealing.[3,4] In spite of the use of powerful techniques like Rutherford backscattering spectrometry (RBS),[4] transmission electron microscopy (TEM),[5] deep-level transient spectroscopy,[6] and electron paramagnetic resonance,[7] the structural evolution of point defects between RT and the onset of {311} defect formation at around 680 °C is still unclear.

Early experiments carried out, for example, on megaelectron volt electron irradiation of silicon, which produces isolated point defects (PDs), allowed a clear understanding of PD interaction as well as their evolution into extended defects. These experiments, the fact that simple PD structures are identifiable by spectroscopy,[8,9] and the development of simulations based on the binary collision approximation (BCA)[10] led to a general interpretation of ion-implantation-related phenomena in terms of PD kinetics. Its validity was reinforced by the success of the "+1 model".[11]

It turns out, however, that the phenomenon is much more complex to describe, at least in its initial stages. Molecular dynamics simulations (MD) demonstrate that complex damage structures, often called "amorphous pockets," are formed during ion implantation of silicon, and their annealing is a process that depends on the details of their structure and their interface with the crystal.[12] One can attempt to define criteria to interpret these structures in terms of vacancies and interstitials,[13] but the general picture emerging from MD simulations is that after low-energy ion implantation, the majority of the damage is actually contained in clusters consisting of tens of atoms[14,15] with no particular ordering. A difficulty with MD simulations is to extend them to experimental timescales in order to precisely take into account effects such as dynamic annealing.

From the experimental point of view, small structures in a background remaining largely crystalline are difficult to observe by direct methods such as TEM, although this is possible for damage tracks produced by very heavy ions.[16] In this case, the annealing is shown to be a complex phenomenon not simply related to the size of the damage zones. It occurs by quick steps, estimated to a few picoseconds by MD simulations.[12]

During the last few years, members of our group have carried out calorimetry on high-energy proton-irradiated and low-energy ion-implanted silicon. Calorimetry provides information on the amount of heat released by the annealing of implantation defects and can be extremely useful for the understanding of mechanisms underlying damage annealing. For proton-irradiated monocrystalline silicon (c-Si), Poirier *et al.* noticed that only a part of the heat released by damage annealing could be related to PD kinetics, with the thermal activation of their mobility resulting in well-defined peaks.[17] More than 50% of the heat release actually takes the form of

 ©2007 The American Physical Society

a uniform background. (It is important to note that while megaelectron volt electrons can transfer a maximum amount of energy just above the displacement energy to Si atoms, producing relatively simple PDs, megaelectron volt protons in Si also generate a significant number of primary knock-ons of tens, or even hundreds of kiloelectron volts and their resulting collision cascade.) For the damage generated by low-energy ion implantation in polycrystalline silicon (poly-Si), we showed that heat is released uniformly over the temperature scan, and that the process does not depend on the implantation fluence.[18] This implies that the same kind of annealing mechanisms occur in isolated cascades as in highly damaged material. The shape of the heat release cannot be described by simple PD kinetics. It is, rather, compatible with the complex and multiple processes associated with the annealing of damage structures such as those predicted by MD. The shape of the heat release is also compatible with another complex phenomenon: the relaxation of implanted amorphous silicon (a-Si).[19,20]

The purpose of this paper is to compare results obtained by nanocalorimetry for different types of silicon implanted with different ions. It is shown that the annealing of damage in low-energy implanted silicon is dominated by the structural changes within the damage zones of each ion, and that these changes actually involve the same mechanisms in the different forms of Si. This interpretation is discussed in the light of channeling, Raman scattering, and reflectometry measurements as well as other results and simulations from the literature.

II. NANOCALORIMETRY

A. Experimental details

1. Nanocalorimetry devices, measurements, and data analysis

Nanocalorimetry works on similar principles as differential scanning calorimetry (DSC), but the low addenda and high scanning rate make the technique sensitive enough to measure, for instance, the heat released by low-energy, low-fluence, ion-implanted silicon.[18] It can be applied *in situ*, opening the door to low-temperature measurements.[20] It has been previously used to look at different nanoscale phenomena such as the melting point depression in nanostructures[21–23] and the glass transition in thin polymer films.[24]

A detailed description of device fabrication and a summary of the data analysis steps can be found in Ref. 25. The device is schematically depicted in Fig. 1. It consists in a thin (150 nm), low-stress amorphous Si_3N_x layer deposited on a silicon wafer by low-pressure chemical vapor deposition supporting a patterned platinum layer (25 nm thick) deposited by sputtering over a 3-nm Ti adhesion layer. On the back side of the wafer, a rectangular opening is made in the wafer by tetramethyl ammonium hydroxide etching. The resulting structure is a rectangular Si_3N_x membrane supported by a Si frame with a Pt strip running through the center of the rectangle. Finally, a 140-nm-thick layer of a-Si is deposited by plasma sputtering on the membrane from the back side using a shadow mask aligned with the Pt strip. Its width is effectively 650 μm, exceeding the heater strip width by ~75 μm from each side,[25] so the total probed area is 4.7 mm^2. For the experiments on a-Si, the nanocalorimeters were used as is. For experiments on poly-Si, the fabrication is followed by a 900 °C anneal for 100 s in a N_2 atmosphere to ensure a good crystallization and to obtain relatively large poly-Si grains. From plan-view TEM (Fig. 2), the average grain size is estimated to about 75 nm. Our experiments are currently limited by our ability to deposit the material under investigation on the membrane: devices with a thin strip of c-Si remaining on the Si_3N_x membrane are under development, but no nanocalorimetry measurements were performed on c-Si.

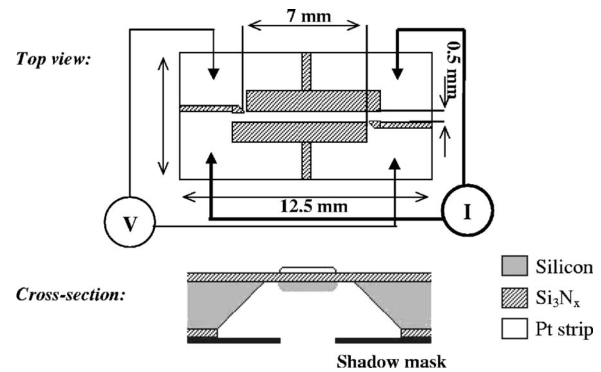

FIG. 1. Planar and cross-sectional views of a nanocalorimeter sensor with poly-Si on the back side (not to scale).

Nanocalorimetry measurements are carried out in differential mode using two nominally identical devices, both with Si deposited on them. One of them is implanted while the other remains intact and serves as a reference. A measurement is initiated by applying a 30-mA current pulse for 10–20 ms through the Pt strip. Resistive heating allows us to increase the temperature at an average rate of 33 000 K/s, turning small amounts of heat into measurable power.

The voltage V and current I across the Pt strip are measured and are used to calculate the heating power (VI). The temperature T of the sensing area is determined by the resistance $R(T)$ of the Pt strip (V/I). The relation $R(T)$ is estab-

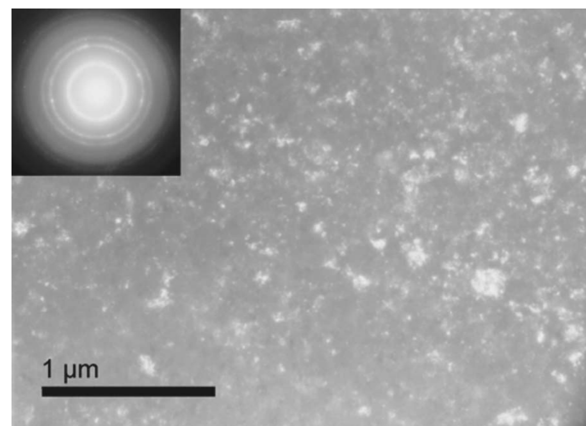

FIG. 2. Dark-field plan-view TEM image of a 140-nm-thick poly-Si layer deposited on a SiN_x membrane at 300 °C and annealed at 900 °C for 100 s. The diffraction pattern appears in the inset.

lished during a calibration procedure by measuring the resistance of the strip as a function of temperature in a slowly cooling furnace under N_2 atmosphere. V is measured by two small contacts located near each end of the strip, but far enough from the ends so the temperature is uniform within 10% between these contacts. Further numerical analysis details of the temperature uniformity can be found in Ref. 26. Uniformity proved to have only a small effect on our measurements.[25]

As material is deposited onto *both* nanocalorimeters, heat capacity should not contribute to the signal. Hence, using the calculation method of Refs. 25 and 27, we can compute the heat rate

$$q(T) = C_P^{impl}(T) + Q(T) - C_P^{ref}(T),$$

where T is the temperature, C_P^{impl} and C_P^{ref} are the nominally identical heat capacity of the implanted and reference nanocalorimeters, respectively, and Q is the rate at which heat is released by damage annealing. Any heat capacity difference between the nanocalorimeters is actually subtracted using a baseline measurement.

The calculation method also involves a correction for the thermal losses that are not exactly the same during an experiment compared to the baseline measurements. Given the very small thermal conductivity of the thin membrane and the absence of convective losses *in vacuo*, only the radiative losses are significant. Short pulses contribute to the minimization of these losses, but because of their temperature dependence ($\sim T^4$), they become a severe problem above 500 °C, introducing overwhelming noise to the measurement. In addition, the $R(T)$ relation is not reliable above approximately 450 °C because conductivity through the Si frame of the devices becomes significant during the calibration procedure. (This effect does not occur during a nanocalorimetry scan because only the Pt strip is heated.) An unreliable $R(T)$ relation may lead to large errors in the amount and the shape of the heat release.[28] For these reasons, presenting results for temperatures above 500 °C (350 °C for low-temperature measurements) could be misleading.

In order to illustrate this point, Fig. 3 shows a nanocalorimetry signal calculated using an extrapolation of the $R(T)$ relation. The details of the shape of the signal are discussed in the results section. It is seen in Fig. 3 that fluctuations in the signal become important above 500 °C and quickly dominate the signal. This is related both to the increasing importance of thermal losses relative to the heat release and to the noise induced by the loss of sensitivity as the heating rate decreases dramatically. Still, the signal fluctuates symmetrically, so there is no evidence that the heat release increases or decreases between 500 °C and 650 °C. A similar uniform heat release is observed by DSC carried out on Si amorphized by self-implantation at megaelectron volt energies,[19] as discussed in the following section. These DSC measurements show a recrystallization peak at 680 °C that could only be guessed in our measurements given the amplitude of the noise. For these reasons, we show only the nanocalorimetry signals for the temperature range for which we have a reliable temperature calibration and a heat release not dominated by noise but based on comparisons with the DSC

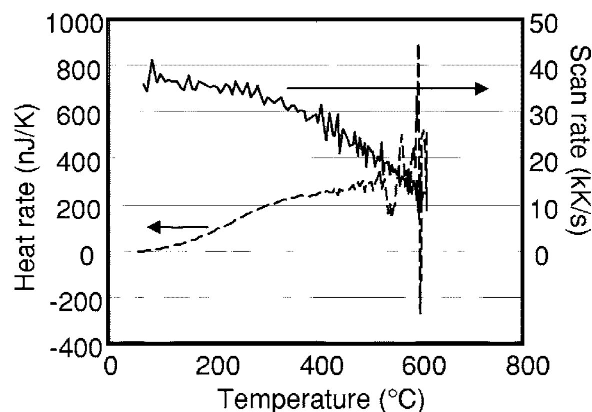

FIG. 3. Example of a complete heat rate measurement (dashed line) and temperature scan rate (solid line) after a 30 keV Si implant in poly-Si at a fluence of 4 Si/nm^2, showing the significant noise appearing in the measurement above 500 °C and the decreasing scan rate, both associated with radiative losses that become significant at high temperature.

measurement, but it is unlikely that the amplitude of the heat release does not remain uniform between 500 and 650 °C.

It is important to underline, though, that the discussion presented here is based on observations of the heat release below 500 °C and on the assumption that the signal remains comparable above this temperature. It is possible that observations above this temperature lead to different conclusions.

2. Ion implantation

Sample and reference nanocalorimeters were placed in the implantation chamber (base pressure of 2×10^{-6} Torr), but only the sample nanocalorimeter was implanted. Low-energy implantations of 30 keV Si^-, 15 keV Si^-, and 15 keV C^- were performed by extracting negatively charged ions from a sputtering source biased at the desired voltage without net acceleration inside a Tandetron accelerator. For the 4 keV He^+ implantation, we used a duoplasmatron source on a low-energy ion implanter. The implantation beam line is equipped with a neutral beam trap. Implantations were carried with a 350 nA current over an area of 17.2 cm^2, either at RT or at low temperature. The ion beam current was monitored during the implantation and was also measured with a Faraday cup before and after a series of implantations to assure that the current did not change during the implantation. Implantations at fluences ranging from 6×10^{-3} to 8 ions/nm^2 were carried out. The uncertainty in the fluences is estimated to be below 10%. For low-temperature measurements, liquid nitrogen was poured into the sample holder and the devices were surrounded by a thermal shield attached to the sample holder, allowing their temperature to decrease to about −150 °C.

In order to compare the results in terms of the amount of accumulated damage, we often express fluences in displacements per atom (DPA). Using SRIM 2003,[10] we calculated in each case the number of displacements per ion and we estimated the depth of the damage zone as the depth at which the implanted ion concentration decreases to 1/2 of the peak concentration. The conversion factor between fluences expressed in ion/nm^2 and DPA can be found in Table I.

TABLE I. Conversion factors used to convert between fluences expressed in ion/nm^2 and DPA.

Beam	30 keV Si	15 keV Si	15 keV C	4 keV He
Implantation depth [nm]	73	40	83	70
Factor [DPA/(ion/nm^2)]	0.1677	0.1695	0.0604	0.0146

At these energies, no ion can go through the 140-nm poly-Si layer and reach the Si_3N_x membrane. 30 keV Si, 15 keV C, and 4 keV He were chosen because their damage depth profiles are similar but obtained with significantly different ion masses. The nanocalorimetry experiments started with 30 scans at different heating rates prior to implantation, which served to determine the heat loss corrections. Ion implantation was carried out and was followed after an ~30-s delay by ten scans during which nanocalorimeters were heated to above 750 °C for the poly-Si sample and to 500 °C for the a-Si samples. This ensured that all processes were annealed out and that damage is fully annealed in poly-Si, while preventing the recrystallization of a-Si. Measurements revealed that no heat was released after the first scan; the signals returned to the initial baseline.[25] Using the calculation method mentioned above, we calculated the rate of heat release by damage annealing after each implantation.

B. Results and discussion

Figure 4 presents the rate of heat release by damage annealing as a function of temperature for different ion species and fluences. The signals of all implants share a number of common characteristics: (i) they show no peak but rather a smoothly evolving signal; (ii) the rate of heat release tends to flatten at high temperature in all cases; (iii) the amplitude increases at a sublinear rate with fluence and tends to saturate above a certain fluence, which is around 4 at./nm^2 for Si implants.

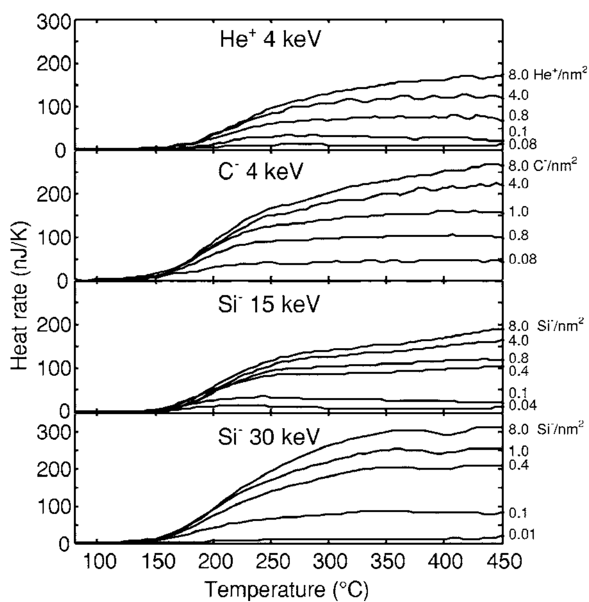

FIG. 4. Heat rate versus temperature for poly-Si implanted with indicated ions and fluences.

The fact that the heat release does not show any peak means that the annealing is characterized by a wide spectrum of processes uniformly distributed in terms of activation energy.[18] Such a wide activation energy distribution is characteristic of the internal relaxation and recrystallization processes of "amorphous pockets." The processes that have small activation energies are promptly activated before the measurement is initiated, causing the signal to be initially null.

One important consequence of the relative uniformity of the rate of heat release is that there should be no correlation between the amount of energy release during an annealing event and the energy barrier that has to be overcome in order for a process to take place. This is reasonable in a context where annealing steps are complex processes involving many atoms. To use an analogy, one can think of a sand pile in which avalanches are observed. The size of an avalanche is not correlated to the difficulty for the first grain of sand to be able to fall. A grain that can easily fall may give rise to a large avalanche, and *vice versa*. Thus, the importance of an event is not related to the difficulty to initiate it. The same may apply to unstable, complex, and various atom configurations for which energy is stored in the form of bond angle distortions and dangling bonds. If, on average, tens or hundreds of atoms are involved in an annealing step, the amount of energy released will not depend on the energy required to move the first atom that initiates this step. Small or large events may be activated at low or high temperature. The only constraint is that since we measure a finite rate of heat release, the energy distribution of the events in terms of released energy must be such that the average energy calculated over this distribution converges, e.g., if it is a power function, its exponent must be smaller than -2, which is not necessarily the case of avalanches. Examples of energy distributions of reconfiguration events for the relaxation of a-Si obtained by simulations can be found in Ref. 29.

It is worth mentioning that uncorrelated activation and released energy distributions are not the only possible explanation. An example of correlated distribution would be to consider that a large proportion of the events have small activation energies but release small amounts of energy, and that much fewer events have large activation energies but release large amounts of energy. However, not only one would then have to identify mechanisms leading to such correlation, but the distributions would have to compensate almost exactly over the energy span, i.e., the product of the number event and their associated energy release must be the same at all activation energies in order to produce a uniform heat release over the temperature scan. (e.g., if the activation energy and the release energy are linearly related, then the number of events and the activation energy must be inversely related, which actually involves two compensating correlations in the system.) We thus consider that the assumption of

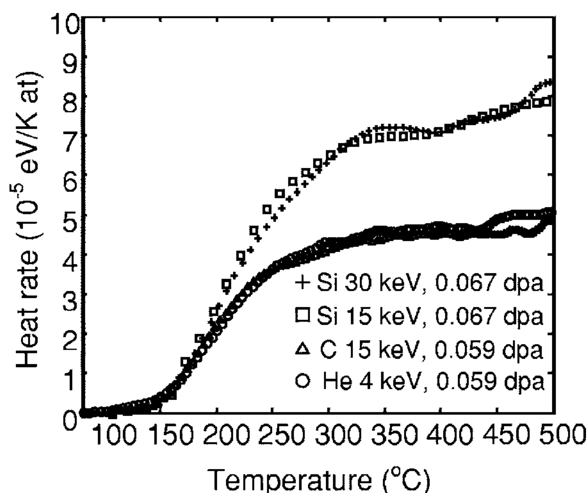

FIG. 5. Heat rate per atom in the implanted zone for poly-Si implanted with 4.0 He^+/nm^2 at 4 keV and 1.0 C^-/nm^2 at 15 keV (0.059 DPA), and with 0.04 Si^-/nm^2 at 15 keV and 0.4 Si^-/nm^2 at 30 keV (0.067 DPA).

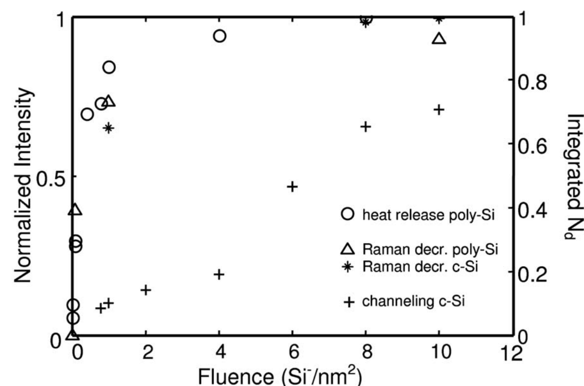

FIG. 6. Raman intensity decrease $(1-I_{imp}/I_{\text{virgin}})$ in poly-Si (triangles) and c-Si (stars) (left scale). Normalized heat release between RT and 500 °C (circles) measured by nanocalorimetry (left scale). Estimated damage in c-Si as obtained from c-RBS (plus) (right scale).

uncorrelated activation and released energies is more reasonable.

In order to identify the influence of ions and energy on the heat release, we plotted for similar fluences, expressed in DPA, the heat rate normalized by the number of atoms in the implanted zone (Fig. 5). We observe that for this similar number of DPA, the results of 15 keV and 30 keV Si^- implantations overlap. This result was expected to some extent since in both cases, we create the same damage concentration per unit volume for the same fluence in DPA, but it makes clear that no surface effects are observable since one implanted region is closer to the surface than the other. For C^- and He^+ implantations, ~40% less heat is released for the same DPA compared to Si^- implantations, but both release heat at the same rate. Clearly, light ions produce damage structures that release significantly less heat than damage produced by heavy ions. There is an evolution in the amount and nature of defects generated between light and heavy ions not taken into account by models based on the binary collision approximation (BCA) such as SRIM. It is a consequence of the fact that Si produces relatively large and concentred damage pockets while light ions produce more sparsely distributed damage, as emphasized by MD simulations.[12,15] The smaller pockets produced by 15 keV C^- and 4 keV He^+ may undergo more dynamic annealing during implantation than the damage produced by 30 keV Si. Consequently, less heat is released during the nanocalorimetry scan. This is in agreement, for example, with measurements by Goldberg *et al.*[30] who show that the critical temperature for amorphization is below RT for C implantations while it is above RT for Si implantation. They attribute this effect to greater dynamic annealing of defects produced by light ions compared to heavier ones at RT. They also show that the critical temperature increases with increasing ion flux, which means that the amorphization is reached at a lower fluence when the implantation current is higher. Interestingly, we found that more heat is released after the same fluence when implanting at a higher current, an effect that we attributed to the stabilization of damage before its dynamic annealing when the ion impact rate is higher.[31]

The present measurements, though, indicate that the mass dependence is not simply related, for example, to the number of displacements per ion. Rather, it exhibits a threshold in terms of ion mass above which damage is produced in such a way that it is more stable during implantation and results in larger heat releases. Meanwhile, the nanocalorimetry signals are at least qualitatively the same for He, C, and Si implantation, so the underlying processes must be similar and involve a wide spectrum of steps and activation energies.

The amount of heat release between RT and 450 °C as a function of the fluence after 30 keV Si implantation is plotted in Fig. 6. We have pointed out that the heat release starts to saturate at around 4 Si^-/nm^2 but is still increasing slowly above this fluence. We attribute this effect to the progressive broadening of the damaged zone with increasingly high fluence,[32] as discussed in the next section.

An important point we want to underline is that the signals obtained from poly-Si are virtually identical to those obtained from the relaxation of implanted a-Si.[20] In Fig. 7, we directly compare the rate of heat release for the two materials after low-temperature implantations of 30 keV Si. It is seen that they only differ in amplitude, the poly-Si releasing less heat than the a-Si. Relaxation in implanted a-Si is characterized by a heat release and a decrease in the width of bond angle distortion distribution during a temperature scan,[19] a process that involves a series of complex structural rearrangements. Each ion impacting a-Si contributes to the increase of these distortions until saturation is reached. The amount of energy that can be stored during the implantation of a-Si reaches that of the recrystallization energy.[20] Given the similar saturation behavior with fluence and the shape correspondence between a-Si and poly-Si, it is clear that damage annealing mechanisms in poly-Si are not different from those involved in the relaxation of a-Si. This leads us to the experimental conclusion that implanted poly-Si does actually contain "amorphous pockets," i.e., that the damage zones in poly-Si are structurally similar to those of implanted a-Si. The signal similarity also implies that the annealing

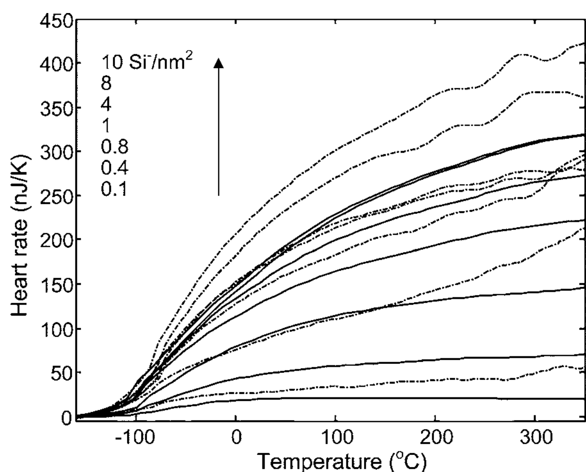

FIG. 7. Rate of heat release by poly-Si (solid lines) and a-Si (dashed-dot lines) implanted at low temperature with 30 keV Si^- at different fluences ranging from 0.1 ions/nm^2 to 10 ions/nm^2.

kinetics in implanted poly-Si are dominated by damage zone relaxation and annealing rather than point defect annealing.

Aside from these common characteristics, however, the signal amplitudes differ significantly between experiments carried out on a-Si and poly-Si. The heat release is higher in the case of a-Si for the same fluence. This behavior was also observed in DSC measurements performed by Roorda *et al.*[19] They measured a smaller heat release for He—implanted c-Si compared to a-Si, except for a fluence of 0.3 DPA for which the heat release is larger for c-Si than for a-Si. Such a light ion at a higher energy may generate a significant number of stable and isolated PDs that will contribute to the heat release. For higher fluences though, the heat release is again smaller in c-Si than in a-Si. Why is the heat release from the crystal smaller? First, isolated and unstable defects produced in crystalline Si will be dynamically annealed so less heat is released during the temperature scan. In a-Si, such a process is less efficient and contributes to the superlinear damage accumulation when c-Si is close to its amorphization.

Another possible contribution is that a process similar to solid phase epitaxy or other type of rearrangement may occur at the surface of the damage zones when they are surrounded by crystalline material, partially healing the material or contributing to a partial relaxation. Such a process, not possible for implanted zones in a-Si, would contribute to a decrease of the energy released during a calorimetry scan. However, after low-temperature ion implantation at high fluence, the poly-Si should be completely amorphized. An effect that we did observe, though, is that the heat release from implanted poly-Si still increases slowly as we reach very high fluences. As already mentioned, we attributed this to the broadening of the amorphized zone which deepens as the fluence increases.[32] So another factor could be the proximity of the crystalline, undamaged substrate that may affect the nearby damage zones.

III. DAMAGE CHARACTERIZATION

We concluded in the previous section that from the calorimetry point of view, the structure of damage zones in all three types of Si and the mechanisms involved in their annealing must be very similar, if not identical. But different types of complex structures may lead to a uniform energy distribution of processes, so the question remains: Is the internal structure of the damage in crystalline Si comparable to a-Si, or at least to the structure of implanted, unrelaxed a-Si? In the second part of the paper, we address the question of the applicability of the proposition by performing optical characterization on both materials and discuss key results from the literature. We will also compare the results obtained by these techniques to the damage accumulation determined by channeling measurements.

A. Optical characterization

Raman scattering is, in principle, a method of choice for assessing the crystallinity of a material, and has been used extensively to characterize the amorphization of Si and to assess the structure of a-Si.[19,33] Reflectometry has also been used extensively to characterize damage accumulation in Si.[34] In order to compare the damage effects in c-Si, poly-Si, and a-Si, we performed both types of analysis on these materials.

Raman spectra were recorded at RT using the 488-nm line from an Ar-ion laser that was scattered from the sample in backscattering geometry and spectrally resolved onto a charge-coupled device (CCD) camera using a double grating spectrometer. Other Ar^+ plasma lines were removed using a prespectrometer monochromator. Exposures were taken for 300 s. In the case of nanocalorimeters, the beam was focused along the strip, and the laser power was reduced to 10 mW to avoid heating. The penetration depth of the laser varies with the degree of damage in the substrate from 800 nm for c-Si to ~40 nm for a-Si.[35] With increasing ion fluence, Raman spectroscopy exhibits a progressive reduction in depth perception.

For optical reflectometry, we performed the measurements *in situ* using a He-Ne laser modulated by a mechanical chopper. The incident and reflected light were detected by two Si photodiodes. Two standard lock-in amplifiers including low-noise preamplifiers were used for signal collection, and their outputs were connected to a PC for control, acquisition, data storage, and graphical presentation of the data. The data for c-Si were obtained from a bulk piece of Si while the poly-Si and a-Si samples were deposited on Si_3N_x membranes under the same conditions as for nanocalorimeter preparation.

1. Raman scattering spectroscopy

Figure 8 shows Raman spectra of the first-order Raman peaks for the poly-Si of a nanocalorimeter (a) and c-Si sample (b) both implanted with 30 keV Si^- at indicated fluences. A reduction in intensity of the first-order Raman peak can be seen as a function of implantation fluence. The spectrum of the unimplanted sample is also shown for comparison (top curve). The c-Si and poly-Si spectra are determined by wave vector selection rules, with the LO peak at 520 cm^{-1} dominating the underlying second-order Raman characteristics. The intensity of this peak is polarization-dependent and is attributed to the creation of triply degenerate, long-wavelength optical phonons.[36]

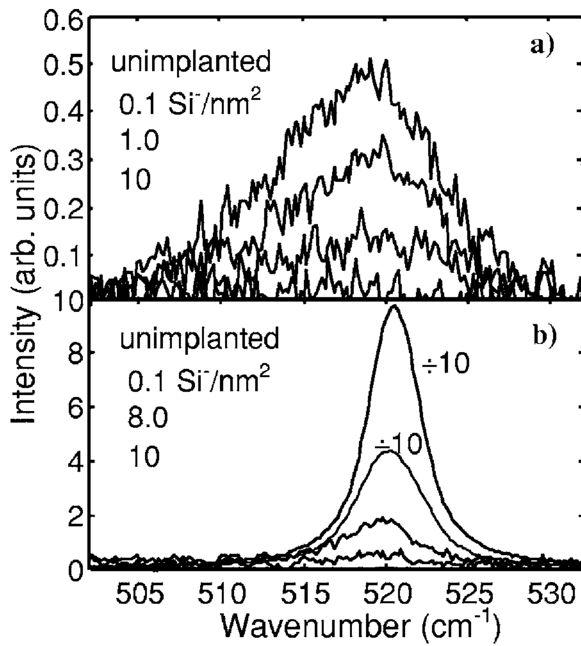

FIG. 8. Raman spectra obtained from poly-Si (top) and c-Si (bottom) unimplanted and implanted with 30 keV Si^- at fluence ranging from 10^{14} to 10^{15} $ions/cm^2$. On poly-Si, the incident power was reduced to avoid heating.

The shape of the peak asymmetrically broadens due to reduced phonon length caused by the phonon confinement. It is thus broader for poly-Si than for c-Si. The reduction in intensity is associated with the increasing amount of damage. This is illustrated in Fig. 6, which shows the reduction in intensity of the Raman peak, $1\text{-}I_{imp}/I_{virgin}$, as a function of fluence. The intensity reduction closely follows the heat release progression with fluence. The very similar trend observed in both c-Si and poly-Si is an indication that damage accumulation occurs at the same rate.

However, because Raman spectroscopy is very sensitive to damage accumulation, no straightforward or proportional link can be made between the intensity and the amount of damage. The intensity decrease may rather be attributed to enhanced absorption or Rayleigh scattering. In order to get more direct information about the change in crystallinity of the two materials, we performed reflectometry measurements.

2. In situ optical reflectometry

Figure 9 shows the normalized fractional change in optical reflectometry ($\Delta R/R_o$) of c-Si and poly-Si as a function of fluence during an implantation at RT. The initial progression is not identical, but the general behavior of both materials is similar as the change in reflectivity saturates at about the same fluence. The normalized $\Delta R/R_o$ saturates at approximately 4 Si/nm^2. In addition, as for Raman measurements, the normalized $\Delta R/R_o$ shows the same progression versus fluence as the heat release. The initial slope is not the same, though, which indicates that damage accumulation is slower in c-Si than in poly-Si and a-Si, probably as a result of more efficient dynamic annealing in a monocrystalline

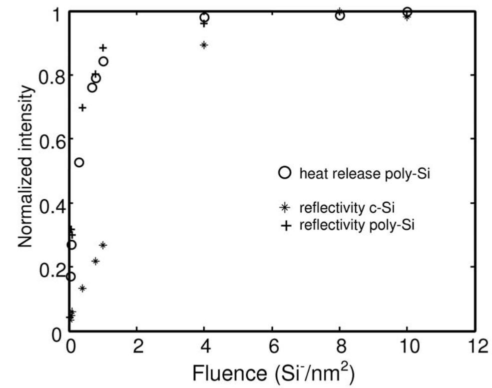

FIG. 9. Normalized fractional change in optical reflectivity ($\Delta R/R_o$) of c-Si (stars) and poly-Si (plus). Normalized heat release between RT and 500 °C (circles) as measured by nanocalorimetry for 30 keV Si^- implanted at room temperature.

material. Since the progression of optical measurements with fluence is similar for all three types of silicon, at least from the saturation behavior point of view, it independently indicates that materials are comparable from the damage accumulation point of view. It also shows that unrelaxation of a-Si by low-energy ion implantation and damage accumulation in poly-Si are comparable processes.

B. General discussion

We have already cited a few key results from the literature, especially calorimetry and simulation work. In the previous section, optical characterization methods led us to conclude that damage accumulation is similar in all three forms of silicon. In this section, we review other supporting evidence for the interpretation that damage zones are structurally similar to a-Si.

From the experimental point of view, Barklie and O'Raifeartaigh[37] recently performed electron paramagnetic resonance (EPR) measurements on ion-implanted Si and suggested that a broad line in the signal, overlooked in previous investigations, is related to these amorphous pockets. They show that these defects are already present after low-fluence implantation and in much larger concentration than other, simpler PD, at least for heavy ion or lower energy ion implantation. Their number increases also sublinearly with fluence, as does the nanocalorimetry signal amplitude.

In an article by Liu *et al.*,[38] it was shown that low-energy localized vibrational excitations, a common feature of amorphous solids, gradually appear in ion-implanted Si, although the material remains largely crystalline. It is illuminating to consider that if the damage zones are structurally similar if not identical to a-Si, then they should behave the same way from the point of view of processes such as low-energy excitations, and give rise to this phenomenon at the same rate as they appear. Again, the increase with fluence is sublinear.

From the numerical simulation point of view, as mentioned earlier, MD predicts the formation of damage zones.[12,14] Recent MD simulations by Santos *et al.*[15] show that the fraction of displaced atoms contained in each dam-

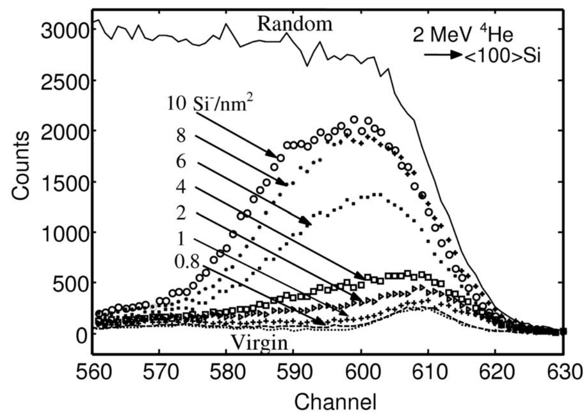

FIG. 10. Channeling spectra from c-Si implanted with 30 keV Si at room temperature at indicated fluences (symbols). The random (solid line) and aligned (dashed line) spectra of unimplanted c-Si are shown for comparison. Spectra were obtained along the ⟨100⟩ axis using 2 MeV $^{4}He^{+}$ ions detected at a scattering angle of 170° to the incident beam axis.

age zone increases with ion mass. Although PDs are generated, all ions form a significant number of clusters or amorphous pockets, most of them consisting of a relatively large number of atoms. The same group also suggests an interpretation of the "amorphous pockets" formation and annealing in terms of interstitial-vacancy mechanisms.[13,39,40] This approach, however, does not necessarily take into account the complex rearrangement process internal to the damage zone associated with annealing steps that release heat and lead to a decrease of the bond angle distortion in a-Si.[20]

C. RBS channeling

We have evidence from reflectometry and the literature that damage accumulation is comparable in different types of Si. The different calorimetry measurements and reports also show a great similarity in the evolution of these defects. In order to correlate the heat release behavior to damage accumulation, we performed RBS in channeling mode on c-Si self-implanted with 30 keV Si at a flux of 70 nA/cm^2 or 4.3×10^{-3}Si/nm^2 s. Channeling measurements were performed by means of a 5 nA beam of 2 MeV He^{+} from a Tandetron accelerator. The beam was aligned along the ⟨100⟩ axis. Spectra were collected with a surface barrier detector placed at a scattering angle of 170° to the incident beam axis.

Figure 10 shows the channeling spectra of samples implanted at RT with 30 keV Si^{-} ions, with fluences from 0.8 to 10 Si/nm^2. The solid line denotes the spectrum obtained from a randomly oriented crystal while the dashed line is that for an aligned, unimplanted crystal. The yield in the channeled spectra is sensitive to atoms in the channel and is observed to increase with increasing fluence. The yield in the implanted region increases monotonically with fluence without reaching the random level. This is compatible with data in the literature, given the relatively small ion flux used during these implantations.[41] A broadening of the damage region is observed for high fluences and can be explained by the creation of complex damage progressively deeper into the substrate.[32]

From the spectra of Fig. 10, the number of displaced atoms N_d was estimated by means of a computer program that uses an iterative procedure to subtract the dechanneling contribution from channeling spectra, assuming the two-beam approximation. N_d is normalized so 1.0 coincides to the random level. The integrated displaced atom fractions obtained in this manner are plotted in Fig. 6 as a function of the implantation fluence. As known from the literature ,[42] damage increases initially at a sublinear rate due to dynamic annealing and then, above 4 Si/nm^2, switches to a superlinear rate that is ascribed to the enhanced capture of defects by amorphous zones. At 8 Si/nm^2, though, the spectrum has not yet reached the random level, which means that at these fluences the crystal is not totally amorphized.

The channeling signal does not follow the evolution of the released heat as measured by nanocalorimetry. A similar behavior was also observed by Roorda *et al.* for light ion implantation at much higher energies.[19] In He-implanted c-Si, the heat release measured by DSC (Ref. 19, Fig. 16b) is already 1/2 of the maximum value and 2/3 of its final value after a fluence of 0.1 DPA, while the damage estimated from channeling (Ref. 19, Fig. 11a) is still fairly small. The heat release reaches a maximum at 0.3 DPA, while channeling indicates that the material is far from being amorphized.

In this context, it can be stated that above 4 Si^{-}/nm^2, when damage accumulation measured by channeling enters its superlinear phase, further damage does not occur at the expense of more stored energy. As channeling indicates that at low fluence a significant fraction of the material remains fairly crystalline, this implies that the system accommodates a small number of structures that store a lot of energy and evolve toward an amorphous structure that stores a similar amount of free energy. At this point, far from equilibrium, it is energetically more favorable for the system to nucleate large-scale amorphous zones than to accommodate more distortions and defects in small amorphous zones.

IV. CONCLUSIONS

Nanocalorimetry experiments carried out in low-energy, self-implanted a-Si and poly-Si show that the heat released during a temperature scan between implantation temperature and 350–500 °C shares important characteristics such a smooth, featureless shape and similar saturation behavior with fluence. The saturation behavior is also reflected in optical characterizations. Considering these results and putting them in perspective with other experimental results[17,19,20,37,38] and simulations[12,14,15] obtained for c-Si leads us to conclude that the annealing of implanted (and dynamically annealed) crystalline silicon is dominated, at least in its initial stages, by the relaxation and the annealing of damage zones that are structurally very similar if not identical to a-Si. This also applies to the primary knock-ons of a few kiloelectron volts generated by light, high-energy ions. The amount of heat released by implanted a-Si is larger than that from poly-Si, which indicates that the surrounding crystal plays a significant role in the formation and dynamic

annealing of such damage zones. Finally, channeling measurements indicate that at the saturation fluence of nanocalorimetry, we are far from amorphization, implying that further damage occurs by structural transformation without the addition of more stored energy.

ACKNOWLEDGMENTS

The authors are grateful to L. H. Allen and M. Yu. Efremov (UIUC) as well as S. Roorda, R. Poirier, N. Mousseau (U. Montréal), A. Yelon (École Polytechnique), and S. Jandl (U. Sherbrooke) for fruitful discussions. Thanks are also due to L. Godbout and R. Gosselin for their excellent technical assistance with the accelerator operation, M. Skvarla and P. Infante of the Cornell Nanofabrication Facility, as well as O. Grenier and S. Bah of the École Polytechnique de Montréal for their assistance with nanocalorimeter fabrication. This work was supported by the Natural Science and Engineering Research Council of Canada, NanoQuébec, and the Fonds Québécois de la Recherche sur la Nature et les Technologies.

*Corresponding author. Email address: francois.schiettekatte@umontreal.ca

[1] P. A. Stolk, H.-J. Gossmann, D. J. Eaglesham, D. C. Jacobson, C. S. Rafferty, G. H. Gilmer, M. Jaraız, J. M. Poate, H. S. Luftman, and T. E. Haynes, J. Appl. Phys. **81**, 6031 (1997).

[2] M. D. Giles, J. Electrochem. Soc. **138**, 1160 (1991).

[3] Jeongnim Kim, Florian Kirchhoff, John W. Wilkins, and Furrukh S. Khan, Phys. Rev. Lett. **84**, 503 (2000).

[4] F. Schiettekatte, S. Roorda, R. Poirier, M. O. Fortin, S. Chazal, and R. Héliou, Nucl. Instrum. Methods Phys. Res. B **164–165**, 425 (2000).

[5] D. J. Eaglesham, V. C. Venezia, H. J. Gossmann, and A. Agarwal, J. Electron Microsc. **49**, 293 (2000).

[6] S. Libertino, S. Coffa, and J. L. Benton, Phys. Rev. B **63**, 195206 (2001).

[7] Young Hoon Lee, Appl. Phys. Lett. **73**, 1119 (1998).

[8] G. D. Watkins and J. W. Corbett, Phys. Rev. **138**, A543 (1965).

[9] L. J. Cheng, J. C. Corelli, J. W. Corbett, and G. D. Watkins, Phys. Rev. **152**, 761 (1966).

[10] J. F. Ziegler, J. P. Biersack, and U. Littmark, *The Stopping and Range of Ions in Solids* (Pergamon Press, New York, 1985).

[11] M. D. Giles, J. Electrochem. Soc. **138**, 1160 (1991).

[12] M. J. Caturla, T. Diaz de la Rubia, L. A. Marqués, and G. H. Gilmer, Phys. Rev. B **54**, 16683 (1996).

[13] L. A. Marqués, L. Pelaz, M. Aboy, L. Enríquez, and J. Barbolla, Phys. Rev. Lett. **91**, 135504 (2003).

[14] K. Nordlund, M. Ghaly, R. S. Averback, M. Caturla, T. Diaz de la Rubia, and J. Tarus, Phys. Rev. B **57**, 7556 (1998).

[15] I. Santos, L. A. Marqués, L. Pelaz, P. López, M. Aboy, and J. Barbolla, Mater. Sci. Eng., B **124–125**, 372 (2005).

[16] S. E. Donnelly, R. C. Birtcher, V. M. Visnyakov, and G. Carter, Appl. Phys. Lett. **82**, 1860 (2003).

[17] R. Poirier, S. Roorda, F. Schiettekatte, M. Lalancette, and J. Zikovsky, Physica B **308–310**, 462 (2001); Rémi Poirier, Sjoerd Roorda, and François Schiettekatte, (unpublished).

[18] R. Karmouch, J.-F. Mercure, Y. Anahory, and F. Schiettekatte, Appl. Phys. Lett. **86**, 031912 (2005).

[19] S. Roorda, W. C. Sinke, J. M. Poate, D. C. Jacobson, S. Dierker, B. S. Dennis, D. J. Eaglesham, F. Spaepen, and P. Fuoss, Phys. Rev. B **44**, 3702 (1991).

[20] J.-F. Mercure, R. Karmouch, Y. Anahory, S. Roorda, and F. Schiettekatte, Phys. Rev. B **71**, 134205 (2005).

[21] S. L. Lai, J. Y. Guo, V. Petrova, G. Ramanath, and L. H. Allen, Phys. Rev. Lett. **77**, 99 (1996).

[22] M. Zhang, M. Yu. Efremov, F. Schiettekatte, E. A. Olson, A. T. Kwan, S. L. Lai, T. Wisleder, J. E. Greene, and L. H. Allen, Phys. Rev. B **62**, 10548 (2000).

[23] M. Yu. Efremov, F. Schiettekatte, M. Zhang, E. A. Olson, A. T. Kwan, R. S. Berry, and L. H. Allen, Phys. Rev. Lett. **85**, 3560 (2000).

[24] Mikhail Yu. Efremov, Eric A. Olson, Ming Zhang, Zishu Zhang, and Leslie H. Allen, Phys. Rev. Lett. **91**, 085703 (2003).

[25] R. Karmouch, J.-F. Mercure, and F. Schiettekatte, Thermochim. Acta **432**, 168 (2005).

[26] R. Taillefer, P. Desjardins, and F. Schiettekatte, in *Proceedings of the First Northeast Workshop on Circuits and Systems* (Montreal, Canada, 2003), p. 129.

[27] M. Yu. Efremov, E. A. Olson, M. Zhang, S. L. Lai, F. Schiettekatte, Z. S. Zhang, and L. H. Allen, Thermochim. Acta **412**, 13 (2004).

[28] J.-F. Mercure, Masters Thesis, Université de Montréal, Montreal, Quebec, Canada (2003).

[29] F. Valiquette and N. Mousseau, Phys. Rev. B **68**, 125209 (2003).

[30] R. D. Goldberg, J. S. Williams, and R. G. Elliman, Nucl. Instrum. Methods Phys. Res. B **106**, 242 (1995).

[31] R. Karmouch, J.-F. Mercure, Y. Anahory, and F. Schiettekatte, Nucl. Instrum. Methods Phys. Res. B **241**, 341 (2005).

[32] K. Nordlund, J. Keinonen, E. Rauhala, and T. Ahlgren, Phys. Rev. B **52**, 15170 (1995).

[33] Battaglia, S. Coffa, F. Priolo, G. Compagnini, and G. A. Baratta, Appl. Phys. Lett. **63**, 2204 (1993).

[34] H. Aharoni and P. L. Swart, Appl. Phys. Lett. **44**, 892 (1984).

[35] R. E Hummel, Wei. Xi, P. H. Holloway, and K. A. Jones, J. Appl. Phys. **63**, 2591 (1988).

[36] V. Paillard, P. Puech, M. A. Laguna, R. Carles, B. Kohn, and F. Huisken, J. Appl. Phys. **86**, 1921 (1991).

[37] R. C. Barklie and C. O'Raifeartaigh, J. Phys. Condens. Matter **17**, S2351 (2005).

[38] X. Liu, P. D. Vu, R. O. Pohl, F. Schiettekatte, and S. Roorda, Phys. Rev. Lett. **81**, 3171 (1998).

[39] P. Lopez, L. Pelaz, L. A. Marqués, I. Santos, M. Aboy, and J. Barbolla, Mater. Sci. Eng., B **114–115**, 82 (2004).

[40] L. A. Marqués, L. Pelaz, J. Hernández, J. Barbolla, and G. H. Gilmer, Phys. Rev. B **64**, 045214 (2001).

[41] P. J. Schultz, C. Jagadish, M. C. Ridgway, R. G. Elliman, and J. S. Williams, Phys. Rev. B **44**, R9118 (1991).

[42] N. Hecking, K. F. Heidemann, and E. te Kaat, Nucl. Instrum. Methods Phys. Res. B **15**, 760 (1986).